applied sciences

MDPI

Article

New Approach of the Variable Fractional-Order Model of a Robot Arm

Marcin Bąkała [1,*], Piotr Duch [1] and Piotr Ostalczyk [2]

[1] The Institute of Applied Computer Science, Lodz University of Technology, 90-924 Lodz, Poland
[2] Faculty of Electrical Engineering, The Institute of Control and Industrial Electronics, Warsaw University of Technology, 00-661 Warsaw, Poland
* Correspondence: marcin.bakala@p.lodz.pl

Abstract: This paper proposes a simple mathematical model based on the variable fractional-order difference equation of a robot arm. The model of the described arm does not consider the impact of the movement of the mobile platform, it was assumed that all degrees of freedom would be taken away from it. The implementation of the task was divided into two stages. First, a mechanical model was developed. In order to estimate the torques of nodal propulsion motors, a description of the components of the Lagrange equation for the considered system, i.e., energy, power, and external interactions, and derivation of the equations of motion of the tested manipulator based on the Lagrange equation was made. An additional criterion was also considered in the selection of drives in the kinematic nodes of the links, which was to set the manipulator in a vertical position at a specific time. Processing the measured data of a robot arm, model parameters were selected, and the order function was chosen. The second stage was a simulation, whose results were compared with the collected data.

Keywords: fractional calculus; fractional order; robot arm; fractional variable difference; pulse width modulation

check for updates

Citation: Bąkała, M.; Duch, P.; Ostalczyk, P. New Approach of the Variable Fractional-Order Model of a Robot Arm. *Appl. Sci.* **2023**, *13*, 3304. https://doi.org/10.3390/app13053304

Academic Editor: Dimitris Mourtzis

Received: 29 January 2023
Revised: 28 February 2023
Accepted: 2 March 2023
Published: 5 March 2023

Copyright: © 2023 by the authors. Licensee MDPI, Basel, Switzerland. This article is an open access article distributed under the terms and conditions of the Creative Commons Attribution (CC BY) license (https://creativecommons.org/licenses/by/4.0/).

1. Introduction

Robots are becoming more and more popular every day. It is hard to find an industry where robots are not used. The most popular form of commonly used robots are robotic manipulators, which are employed in the industry to perform repetitive tasks, search and rescue missions [1], and inspections [2]. In the case of robot arms, the most popular approaches are derived from Euler–Lagrange equations [3]. Their complexity, expressed by many relevant parameters, is often difficult to estimate, forcing a search for new solutions. Another new approach to modelling dynamics is based on fractional calculus.

The concept of fractional calculus is not new and has been known since 1695, but it has recently gained popularity as a tool generalizing the commonly known calculus. It is becoming more and more popular in different research areas, ranging from electrical engineering, electromagnetism, electrochemistry, electronics, mechanics, and rheology to biophysics and economy [4–6]. Fractional calculus is also used to solve real-life problems, like control of autonomous vehicles [7], or to model and predict new cases of the COVID-19 [8]. In many instances fractional calculus allows modeling of the dynamics of more complex processes than their integer counterparts [9], for example, in the description of the transient behavior of a robot arm. The fractional system perspective in the study of the PRR (planar parallel robot) with three DOFs (degrees of freedom) was presented in [10]. Fractional calculus also has a generalization; when order varies with time, it is called variable fractional-order (VFO) calculus [11,12].

The concept of variable fractional-order integrals, and differentials was first proposed in 1993 [13]. Some complex physical phenomena show variable fractional order integrators, or differentiator properties [14]. Variable fractional-order calculus was implemented in

many different fields. The increasing attention on theoretical analysis and physical modeling using VFO can be noticed. The experimental study of variable fractional-order differentiators and integrators was examined in [14]. Additionally, the viscoelasticity behavior of rubbery state polymers was modeled using variable fractional-order calculus [15]. The comparison of the prediction of the proposed VFO model and those previously published in the literature demonstrated the higher accuracy of the former. VFO calculus is top-rated in control problems. A study was conducted comparing variable fractional-order PID (VFOPID) controllers for different types of unstable order derivatives [16]. The VFOPID controllers opened new possibilities for shaping its transient characteristics [17–19]. The simulation results of the VFOPID controller applied to plants with delay showing its advantage over both traditional and fractional-order PID controllers [20]. The VFOPID also provides additional flexibility during the designing phase. Another version of controllers which can be enhanced by VFO is fuzzy PID controllers [21]. The variable fractional-order fuzzy PID (VFOFPID) controller was applied along with an active tuned mass damper to improve building structures' performance when subjected to horizontal ground motions [22].

In the paper, we propose a simple model of a robot arm using a variable fractional-order difference equation. In the previous studies, the variable fractional-order discrete-time PD controller for this arm was proposed [16,23] along with the analysis of order function selection [24]. The variable fractional-order backward difference is introduced in Section 2. Next, the description of the robot arm is provided along with a discussion concerning its mathematical models. Then, some rules for the choice of the differentiation order functions are given. Finally, measured and simulated step responses of the robot arm are presented.

2. Mathematical Preliminaries

This Section presents essential information concerning the essential mathematical tool used in mathematical model building [3]. The derivative of the fractional order derivative called further fractional derivative is defined as an approximation of the following series [25–27].

$$\ldots, \int_a^t \int_a^{\tau_1} \int_a^{\tau_2} f(\tau_3) d\tau_3 d\tau_2 d\tau_1, \int_a^t \int_a^{\tau_1} f(\tau_2) d\tau_2 d\tau_1, \int_a^t f(\tau_1) d\tau_1 f(t), \tag{1}$$

$$\frac{df(t)}{dt}, \frac{d^2 f(t)}{dt^2}, \frac{d^3 f(t)}{dt^4}, \ldots$$

In a Davis notation for any real function, $f(t)$ the fractional derivative is denoted as

$$_{t_0}D_t^{(\nu)} f(t), \tag{2}$$

where

t_0, t—terminals of fractional differentiation,
$\nu \epsilon$R—fractional order.

The $_{t_0}D_t^{(-\nu)} f(t)$ notation represents an integral of fractional order.

2.1. Grünwald–Letnikov Definition

For a given function $f(t) \epsilon$R of a real variable t, the first-order left derivative has the form

$$f'(t) = \frac{df(t)}{dt} = \lim_{h \to 0} \frac{f(t) - f(t-h)}{h}, \tag{3}$$

The second-order left derivative is as follows

$$\begin{aligned} f''(t) &= \frac{d^2 f(t)}{dt^2} = \lim_{h\to 0} \frac{f'(t)-f'(t-h)}{h} \\ &= \lim_{h\to 0} \frac{\frac{f(t)-f(t-h)}{h} - \frac{f(t-h)-f(t-2h)}{h}}{h} \\ &= \lim_{h\to 0} \frac{f(t)-2f(t-h)+f(t-2h)}{h^2} \\ &= \lim_{h\to 0} \frac{1}{h^2}[1 \ -2 \ 1] \begin{bmatrix} f(t) \\ f(t-h) \\ f(t-2h) \end{bmatrix}, \end{aligned} \tag{4}$$

For any order n, one has

$$f^{(n)}(t) = \frac{d^n f(t)}{dt^n} = \lim_{h\to 0} \frac{1}{h^n} \begin{bmatrix} a_0^{(n)} & a_1^{(n)} & \cdots & a_n^{(n)} \end{bmatrix} \begin{bmatrix} f(t) \\ f(t-h) \\ \vdots \\ f(t-nh) \end{bmatrix}, \tag{5}$$

or

$$f^{(n)}(t) = \frac{d^n f(t)}{dt^n} = \lim_{h\to 0} \frac{1}{h^n} \sum_{i=0}^{n} a_i^{(n)} f(t-hi), \tag{6}$$

where the coefficients $a_i^{(n)}$ are defined as follows

$$a_i^{(n)} = \begin{cases} 1 & for \quad i = 0 \\ (-1)^i \frac{n(n-1)(n-2)\cdots(n-i+1)}{i!} & for \quad i = 1, 2, 3, \cdots \end{cases} \tag{7}$$

or

$$a_i^{(n)} = a_{i-1}^{(n)} \left(1 - \frac{n+1}{i}\right), \tag{8}$$

The above formulas are valid for any order including fractional ones. Then, one has

$${}_{t_0}D_t^{-n} f(t) = \lim_{h\to 0} h^{-n} \sum_{i=0}^{\frac{t-t_0}{h}} a_i^{(-n)} f(t-hi) = \frac{1}{(n-1)!} \int_{t_0}^{t} (t-\tau)^{n-1} f(\tau) d\tau, \tag{9}$$

The variable fractional-order backward difference (VFOBD) of a bounded discrete function f_k is defined as follows:

$${}_0^{GL}\Delta_k^{(\nu_k)} f_k = a_k^{(\nu_k)} * f_k = \sum_{i=0}^{k} a_i^{(\nu_k)} f_{k-i}, \tag{10}$$

where

$$a_k^{(\nu_k)} = \begin{cases} 0 & for \quad k < 0 \\ 1 & for \quad k = 0 \\ (-1)^k \binom{\nu_k}{k} & for \quad k \geq 1 \end{cases}, \tag{11}$$

$$\binom{\nu_k}{k} = \frac{\nu_k(\nu_k-1)(\nu_k-2)\cdots(\nu_k-k+1)}{k!}, \tag{12}$$

$v_k - order\ of\ the\ fractional\ difference\ in\ the\ time\ step\ k.$

On the basis of the above equations, one derives a general formula

$$\begin{bmatrix} a_0^{(n)} & a_1^{(n)} & \cdots & a_{n-1}^{(n)} & a_n^{(n)} \end{bmatrix} = \begin{bmatrix} a_0^{(n-m)} & a_1^{(n-m)} & \cdots & a_{n-1}^{(n-m)} & a_n^{(n-m)} \end{bmatrix} \begin{bmatrix} a_0^{(m)} & a_1^{(m)} & a_2^{(m)} & a_3^{(m)} & \cdots & 0 & 0 & 0 \\ 0 & a_0^{(m)} & a_1^{(m)} & a_2^{(m)} & \cdots & 0 & 0 & 0 \\ 0 & 0 & a_0^{(m)} & a_1^{(m)} & \cdots & 0 & 0 & 0 \\ 0 & 0 & 0 & a_0^{(m)} & \cdots & 0 & 0 & 0 \\ \vdots & \vdots & \vdots & \vdots & & \vdots & \vdots & \vdots \\ 0 & 0 & 0 & 0 & \cdots & a_0^{(m)} & a_1^{(m)} & a_2^{(m)} \\ 0 & 0 & 0 & 0 & \cdots & 0 & a_0^{(m)} & a_1^{(m)} \\ 0 & 0 & 0 & 0 & \cdots & 0 & 0 & a_0^{(m)} \end{bmatrix}, \tag{13}$$

Equation (13) denotes a discrete convolution and $\nu_k > 0$ is the differentiation order function. For negative order functions, Equation (10) defines variable fractional-order integration (discrete summation). One should realize that for integer order $\mathbb{Z}_+ \ni \nu_k = n > 0$, one immediately obtains a classical backward difference.

$$ {}_0^{GL}\Delta_k^{(n)} f_k = a_k^{(n)} * f_k = \sum_{i=0}^{k} a_i^{(n)} f_{k-i} = \Delta^{(n)} f_k, \tag{14}$$

The above difference may serve as an approximation of a left derivative.

$$\frac{d^n f(t)}{dt^n} = \left.\frac{d^n f(t)}{dt^n}\right|_{t=hk} \approx \frac{{}_0^{GL}\Delta_k^{(n)} f_{kh}}{h^n} = \frac{1}{h^n}\sum_{i=0}^{k} a_i^{(n)} f_{kh-ih} = \frac{\Delta^{(n)} f_k}{h^n}, \tag{15}$$

2.2. The Fractional Order Integrator

As in classical integer order dynamical systems case, on a base of derivatives, one can build differential equations. The simplest one is an equation describing the fractional integrator. So in the fractional systems case,

$$y(t) = T_{u0} D_t^{-v} u(t), \tag{16}$$

where *y(t)* and *u(t)* such that *u(t)* for $t < 0$ denote the system output and input signals, respectively. ν is an order of the integrator whereas $0 < T_u \in R$ is a time constant. For a zero initial condition, the one-sided Laplace transform is of the form which can be further represented by its transfer function.

$$G_{FI}(s, T_u) = \frac{Y(s)}{U(s)} = \frac{1}{T_u s^\nu}\,, \tag{17}$$

The impulse response is described as

$$g_D(t, T_u) = \mathcal{L}^{-1}\{G_{FI}(s, T_u)\} = \mathcal{L}^{-1}\left\{\frac{1}{T_u s^\nu}\right\} = \frac{1}{T_u}\frac{t^{\nu-1}}{\Gamma(\nu)}, \tag{18}$$

where $\Gamma(\nu)$ is the Euler gamma function. The unit step response is described as follows

$$h_D^{(\nu)} I(t) = \mathcal{L}^{-1}\left\{\frac{1}{s} G_{FI}^{(\nu)}(s, T_u)\right\} = \mathcal{L}^{-1}\left\{\frac{1}{T_u(s^{\nu+1})}\right\} = \frac{t^{-\nu}}{\Gamma(1-\nu)}, \tag{19}$$

The fractional integrator response to any signal can be described by an integral

$$y(t) = \int_0^t \frac{\theta^{-\nu-1}}{\Gamma(-\nu)} u(t-\theta)d\theta = \int_0^t \frac{(t-\theta)^{-\nu-1}}{\Gamma(-\nu)} u(\theta)d\theta, \tag{20}$$

2.3. Fractional Derivative

In this subsection, one considers the formula

$$f_h^{(\nu)}(t) = \frac{1}{h^\nu}\sum_{i=0}^{\frac{t-t_0}{h}} a_i^{(\nu)} f(t-hi) = \frac{1}{h^\nu}\begin{bmatrix} a_0^{(\nu)} & a_1^{(\nu)} & \cdots & a_{n-1}^{(\nu)} & a_n^{(\nu)} \end{bmatrix}\begin{bmatrix} f(t) \\ f(t-1h) \\ \vdots \\ f(t-nh+h) \\ f(t-nh) \end{bmatrix}, \quad (21)$$

where $\nu \in \mathbb{R}_+$, $h > 0$ and $n = E\left(\frac{t-t_0}{k}\right)$ is an integer part of a number. Based on the above formula, one defines a fractional order derivative. It is called the Grünwald–Letnikov fractional order derivative [16].

$${}_{t_0}D_t^{(\nu)} f(t) = \lim_{h\to 0} f_h^{(\nu)}(t) = \lim_{h\to 0} \frac{1}{h^\nu}\sum_{i=0}^{\frac{t-t_0}{h}} a_i^{(\nu)} f(t-hi), \quad (22)$$

Fractional Derivative Selected Properties

Fractional derivative linearity property for two differentiable functions $f_1(t)$, $f_2(t)$ and constants a_1, a_2, there is

$${}_{t_0}D_t^{\nu}[a_1 f_1(t) + a_2 f_2(t)] = a_1 {}_{t_0}D_t^{\nu}[f_1(t)] + a_2 {}_{t_0}D_t^{\nu}[f_2(t)], \quad (23)$$

The fractional derivative superposition property for any

$${}_{t_0}D_t^{\nu_1+\nu_2}[f(t)] = {}_{t_0}D_t^{\nu_1}\left\{{}_{t_0}D_t^{\nu_2}[f(t)]\right\} = {}_{t_0}D_t^{\nu_2}\left\{{}_{t_0}D_t^{\nu_1}[f(t)]\right\}, \quad (24)$$

3. The Robot Arm Description

The presented solution is an element of building a comprehensive simulation environment for the robot's actuator in the form of an arm. The study of the system properties is primarily associated with the possibly precise reconstruction of the actual course of the arm's work. Mathematical models are used for this purpose. The model of the described arm does not consider the impact of the movement of the mobile platform, and it was assumed that all degrees of freedom would be taken away from it. The motion system of the presented arm is a simple open kinematic chain, in which the adjacent members relate to each other by means of a kinematic pair. The movement of individual links is independent, performed using dedicated harmonic gears with the ability to maintain a specific position. The mechanical structure of the robot arms allows for their further expansion. The modularity of the structure allows it to quickly change its configuration with no necessity to modify the operation of the entire system. The observation head can be replaced with a gripper or a specialized tool or supplemented with further links. The assumed possibilities of further expansion of the mechanical structure allow for its adaptation to the requirements of the future user, both in the defense and civil operations zone. The whole construction is controlled by a microprocessor system with implanted algorithms using original control procedures with controllers with variable non-integer orders of differentiation. They are a generalization of classical PD regulators. Regulators of this type can be included in the so-called adaptive regulators, where the variables are not so-called controller settings but differentiation and summation orders. Before commencing the work regulation process, appropriate executive systems had to be selected. During the numerical simulations, the following values of the manipulator parameter were assumed:

- m1 = 1.0 [kg]—the weight of the drive systems;
- m2 = 7.0 [kg]—total weight of the manipulator;
- m = 0.5 [kg]—weights of the manipulator links;
- l = 0.5 [m]—the length of the manipulator links;

- $M_0(t)$, $M_1(t)$—driving torque.

Selected ranges of displacements φ_1, and φ_2 of the manipulator links in the given time interval Δt were subjected to numerical analysis in the context of selecting the values and time courses of the drive torques required to complete the given trajectory of the manipulator links. Two basic cases of the initial positions of both links were considered. The calculations assumed the same time course, presented in Figure 1, for changes in the moments $M_0(t)$, $M_1(t)$, where:

- M_0, M_1—fixed values of driving torque;
- Δt_0—start-up phase, an increase of drive torques to the assumed fixed values;
- Δt_1—phase of steady drive torques;
- Δt_2—phase of reduction of drive torques to zero;
- Δt_3—stop phase drive torques equal zero;
- l = 0.5 [m]—the length of the manipulator links.

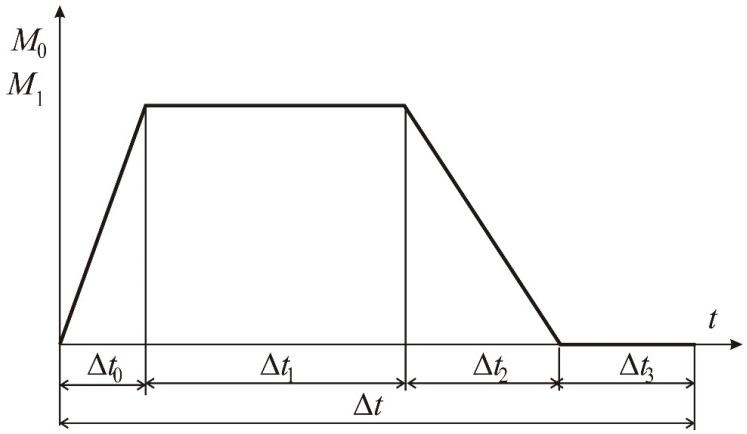

Figure 1. The time course of the moment changes $M_0(t)$, $M_1(t)$.

During the analysis, two prominent cases were studied (Figure 2a,b), mainly setting manipulators in the horizontal and vertical orientation. The first analyzed case is to set the manipulator in vertical position $\varphi_1 = \pi/2$, $\varphi_2 = \pi/2$ (Figure 2b) starting from horizontal position $\varphi_1 = 0$, $\varphi_2 = \pi$ (Figure 2a) in time $\Delta t = 1$ [s].

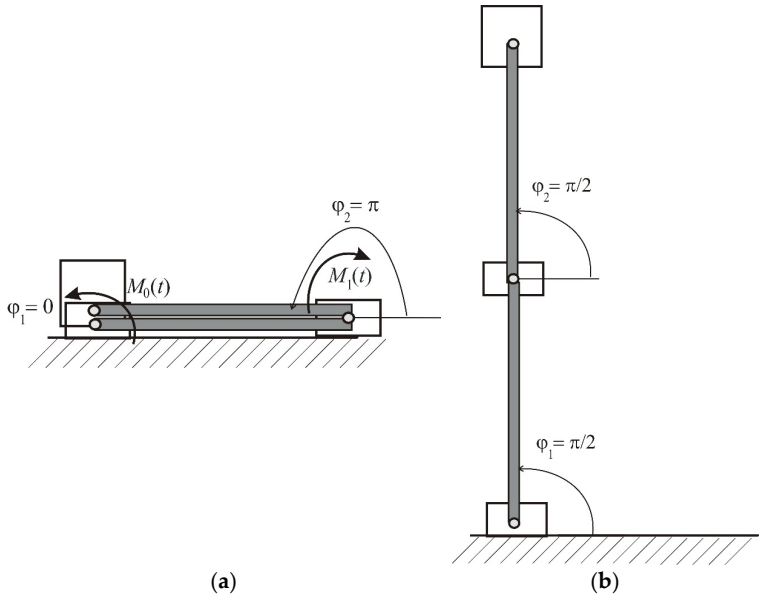

Figure 2. The extreme position of the manipulator's arms: (**a**) folded; (**b**) maximum reach.

From the application point of view, it is important to achieve the required position of the links with the minimum possible values of velocities and accelerations to stop the manipulator. In order to achieve the optimal effect, the following links position and speed functions were considered during numerical simulations:

$$f(x) = \left(\varphi_1 - \frac{\pi}{2}\right)^2 + \left(\varphi_2 - \frac{\pi}{2}\right)^2, \tag{25}$$

$$f(v) = \dot{\varphi}_1^2 + \dot{\varphi}_2^2, \tag{26}$$

When a function (25) reaches the minimum value of zero, the vertical position of the links is realized (Figure 2b). On the other hand, the minima of the function (26) indicate the lowest possible velocities of the manipulator links after a given time Δt. Figure 3a,b show three-dimensional projections of surfaces representing the functions *f(x)* and *f(v)* over the two-dimensional space of parameters M_0, and M_1, while Figure 4a,b shows (in red) areas of these parameters, where functions (25) and (26) reach minimum values. The calculations were carried out by numerically integrating the equations of motion using the 4th order Runge–Kutta method. The time values of the drive parameters (Figure 1) are $\Delta t_0 = 0.05$ [s], $\Delta t_1 = 0.45$ [s], $\Delta t_2 = 0.30$ [s], and $\Delta t_3 = 0.20$ [s].

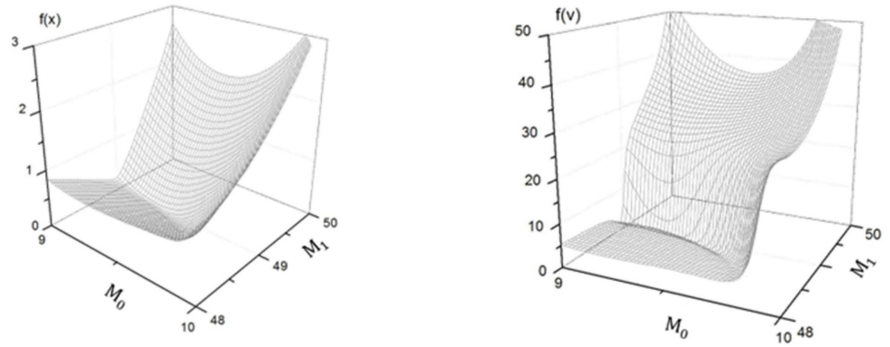

(**a**) (**b**)

Figure 3. Three-dimensional projections of surfaces representing functions f(x) and f(v) over the two-dimensional parameter space M_0, M_1. (**a**) Three-dimensional projections of surfaces representing f(x) functions over the two-dimensional parameter space M_0, M_1. (**b**) Three-dimensional projections of surfaces representing f(v) functions over the two-dimensional parameter space M_0, M_1.

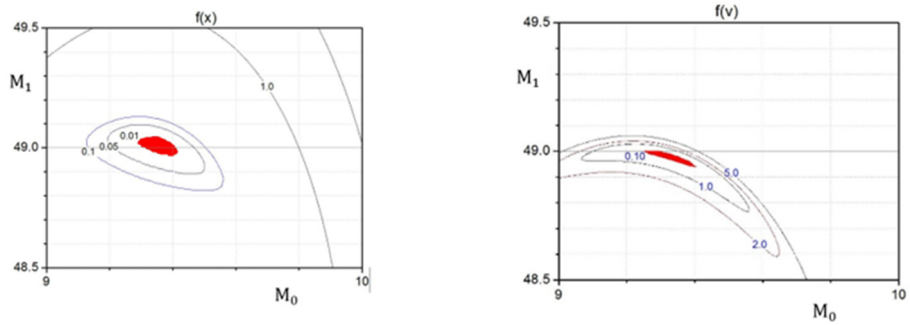

(**a**) (**b**)

Figure 4. The red color indicates areas of these parameters where f(x) and f(v) reach minimum values. (**a**) The areas of parameters M_0 and M_1 where f(x) reaches minimum values. (**b**) The areas of parameters M_0 and M_1 where f(v) reaches minimum values.

The time intervals of the driving torques were selected based on numerical analysis, which was carried out at the fixed values $M_0 = 9.0$ [Nm], $M_1 = 48.0$ [Nm], and the constant on start-up phase $\Delta t_0 = 0.05$ [s]. However, the parameters Δt_1 and Δt_2 changed during

analysis (Δt_3 is the result of select the remaining intervals). The results of this numerical experiment are presented in Figure 5a,b, where the quantities f(x) and f(v) are given as a function of the time intervals Δt_1 and Δt_2. It can be seen that the possibly low-speed values (green areas in the bottom left of the diagram) in Figure 5b coincide with the range where the manipulator reaches the vertical position (green stripe in Figure 5a).

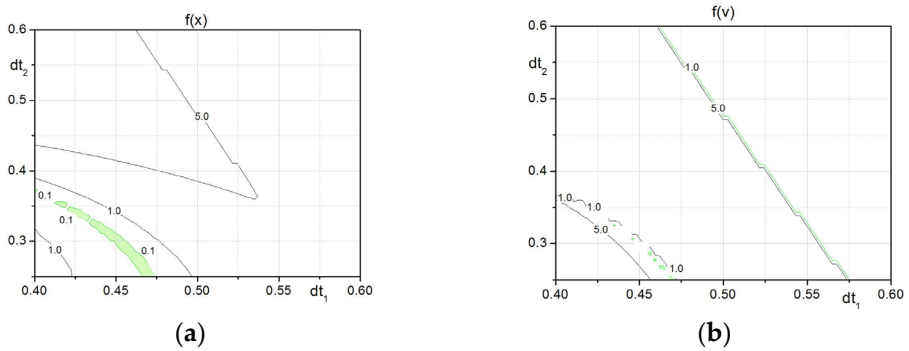

Figure 5. The results of this numerical experiment, where the values f(x) and f(v) are presented as a function of the time intervals Δt_1 and Δt_2. (**a**) The values f(x) is presented as a function of the time intervals Δt1 and Δt2. (**b**) The values f(v) is presented as a function of the time intervals Δt1 and Δt2.

In the last phase of movement, Δt_3 the drive is switched off. Such control of drive torques allows us to achieve the lowest possible values of velocities and angular accelerations when the manipulator links reach the vertical position. This fact is confirmed by the time courses of displacements, velocities, and accelerations presented in Figure 6. The determined driving torques are M_0 = 9.46 [Nm] and M_1 = 49.44 [Nm]. These moments deviate slightly from the optimal values resulting from Figure 4a,b (areas marked in red). The reason for this slight discrepancy may be a different method (Euler's algorithm) or the step of integration of the equations of motion in the case of the diagrams shown in Figure 6. It can be seen that at Δt = 1.0 [s] the cells occupy the required vertical position $\varphi_1 = \varphi_2 = \pi/2$ at relatively low values of velocities and accelerations (Figure 6).

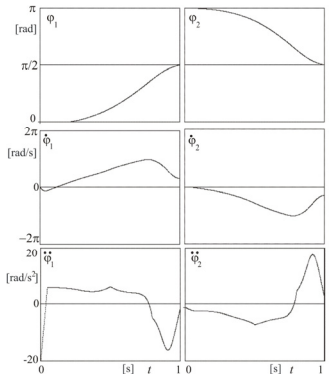

Figure 6. Time waveforms of displacements, velocities, and accelerations.

Figure 7 shows the results of the numerical analysis analogous to the one shown in Figure 6, but taking into account the trajectory limitation of the links by the presence of the base. Contact with the ground means that the first link cannot occupy positions defined by a negative angle φ_1. Hence, when integrating equations, an additional condition was introduced in the form "if $\varphi_1 < 0$ then $\varphi_1 = 0$, $\dot{\varphi}_1 = 0$". The application of this condition allowed us, for the assumed Δt and the vertical position of the links (Figure 7), to obtain the optimal values (Figure 7) at slightly lower values for the drive torques M_0 (8.89 Nm) and M_1 (48.27 Nm).

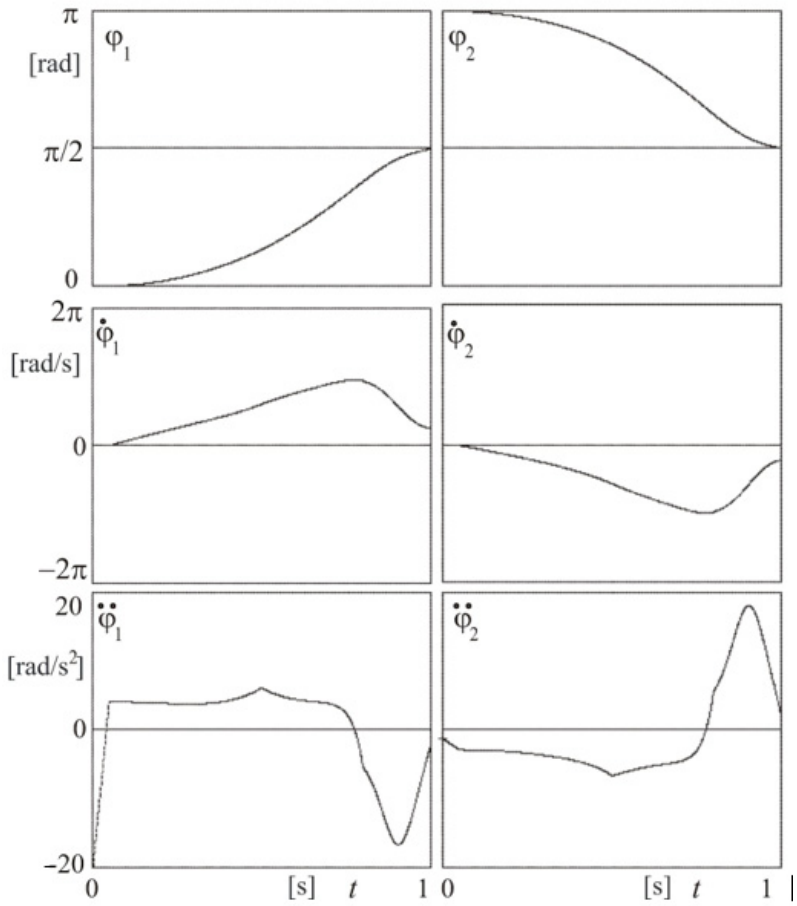

Figure 7. Results of numerical analysis analogous to those shown in Figure 6 but considering the limitation of the trajectory of the links by the presence of the substrate.

The second of the considered cases is shown in Figure 8. The task is to set the manipulator in a vertical position $\varphi_1 = \pi/2$, $\varphi_2 = \pi/2$ (Figure 2b) from the initial horizontal position $\varphi_1 = 0$, $\varphi_2 = 0$ of the links (Figure 8).

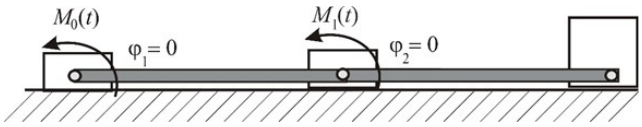

Figure 8. View of the arm in a horizontal position.

Numerical experiments have shown that an attempt to place the manipulator with positively directed moments $M_0(t)$, $M_1(t)$ (Figure 8) requires the application of a maximum torque of at least $M_0 \approx 90$ [Nm] in node "0", both in the case of operation of both drives, as well as in the case of applying only the $M_0(t)$ moment with the locked node "1". On the other hand, the driving power demand is much lower when lifting the manipulator in stages, i.e., moving the link 1 from the position $\varphi_2 = \pi/2$ (Figure 8) to the position $\varphi_2 = 0$ in the first stage, using only the drive $M_1(t)$, and then setting the links in a vertical position in accordance with the case 1 described above, using both drives.

Setting the link 2 in a vertical position (with the locked link 1) with a driving torque of a fixed value $M_1 = 42.4$ [Nm] in time $\Delta t = 1.0$ [s] is shown in Figure 9. The time intervals of the torque M_1(t) are: $\Delta t_0 = 0.05$ [s], $\Delta t_1 = 0.75$ [s], $\Delta t_2 = 0.20$ [s], $\Delta t_3 = 0.0$ [s].

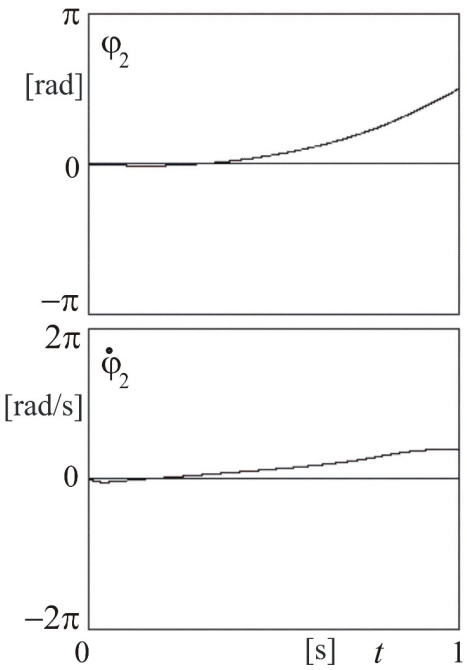

Figure 9. Setting link 2 in a vertical position (with link 1 blocked) with a steady state torque of M_1 = 42.4 [Nm] at time Δt= 1.0 [s].

Figure 10 presents a block diagram of the mathematical model of the robot arm. The arm work is modeled as a simple first-order integrator with negative feedback generated by the moment caused by the gravitational force of the robot arm. Thanks to the use of harmonic gears in the electromagnetic brake in the kinematic nodes, the dynamics of motion can be simplified to the presented model. The correctness of adopting the simplified model can be proven by the presented transient states of the actuator of the described object.

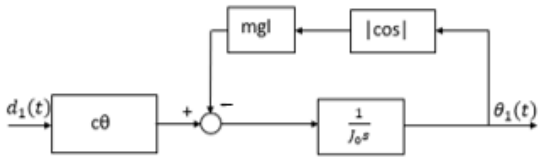

Figure 10. Robot first arm with a motor and shaft block diagram.

Connecting to the inverter positive feedback with a one-step delay block causes the PWM inverter to work as a discrete-time integrator. In order to protect the system against doubled integrating action in the robot arm angular velocity control loop, one introduces additional negative feedback with the discrete differentiation to obtain a closed-loop system treated. Figure 11 presents the block diagram of the first robot arm angular velocity control system.

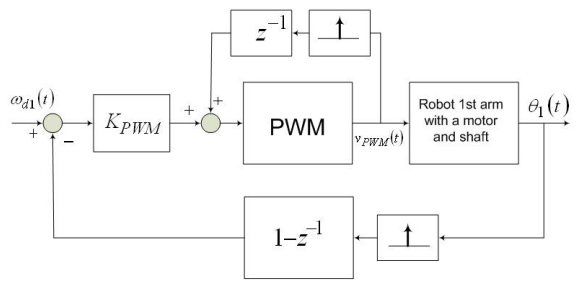

Figure 11. The block diagram of the first robot arm angular velocity control system.

4. The Robot Arm's Mathematical Models

To design optimal manipulator control algorithms, it is necessary to prepare a correct mathematical model describing it [28]. The trade-off between model accuracy and its complexity should also be taken into consideration. In this section two mathematical models of the robot arm are analyzed. The first one is derived from the well-known Newton—Euler formalism whereas in the second the Fractional Calculus is applied. To simplify the calculation model, it was assumed that the mobile platform on which the arm is located is stationary. In addition, the horizontal position of the trolley was assumed, as well as a non-deformable suspension.

4.1. Classical Mathematical Model (CM) of the Robot Arm

The theoretical model of a robot arm is presented in Figure 12 [6,10].

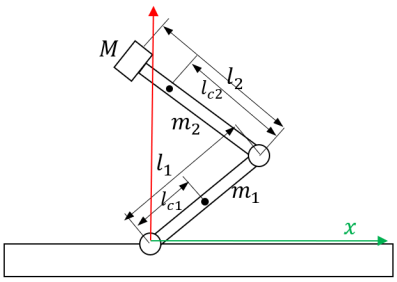

Figure 12. The theoretical model of robot arm.

Following the Euler–Lagrange formalism, two classical differential second-order equations describing the dynamic system are as follows

$$D[q(t)]\ddot{q}(t) + C\left[q(t), \dot{q}(t)\right]\dot{q}(t) + g[q(t)] = \tau(t) \tag{27}$$

where

$$\tau(t) = \begin{bmatrix} \tau_1(t) \\ \tau_2(t) \end{bmatrix} - \text{drive moments},$$

$$q(t) = \begin{bmatrix} q_1(t) \\ q_2(t) \end{bmatrix} - \text{coordinates of the manipulator links position},$$

$$D[q(t)] = D = \begin{bmatrix} I_1 + I_2 & I_2 \\ I_2 & I_2 \end{bmatrix} - \text{moments of inertia matrix of the driving system},$$

$$C\left[q(t), \dot{q}(t)\right] = \begin{bmatrix} h(t)\dot{q}_2(t) & h(t)\dot{q}_2(t) + h(t)\dot{q}_1(t) \\ -h(t)\dot{q}_1(t) & 0 \end{bmatrix} =$$

$$= m_2 l_1 l_{c2} sin[q_2(t)] \begin{bmatrix} -\dot{q}_2(t) & -\dot{q}_2(t) - \dot{q}_1(t) \\ \dot{q}_1(t) & 0 \end{bmatrix},$$

$$h(t) = -m_2 l_1 l_{c2} sin[q_2(t)],$$

$$g[q(t)] = g \begin{bmatrix} (m_1 l_{c1} + m_2 l_1) cos[q_1(t)] + m_2 l_{c2} cos[q_1(t) + q_2(t)] \\ m_2 l_{c2} cos[q_1(t) + q_2(t)] \end{bmatrix},$$

g—acceleration of the Earth,
l_1, l_2—lengths of the robot arm,
l_{c1}, l_{c2}—distance from the precedent joint to the arm centroid.

Now one assumes that the second arm is immobilized. This means that $\ddot{q}_2(t) = 0$,

$\dot{q}_2(t) = 0$, and $q_2(t) = q_2 = \text{const}$, $\tau_2(t) = 0$. From Equation (27), one obtains

$$\begin{bmatrix} I_1 + I_2 & I_2 \\ I_2 & I_2 \end{bmatrix} \ddot{q}(t) + \dot{q}_1(t) m_2 l_1 l_{c2} sin[q_2] \begin{bmatrix} 0 & -1 \\ 1 & 0 \end{bmatrix} \dot{q}(t) + g \begin{bmatrix} (m_1 l_{c1} + m_2 l_1) cos[q_1(t)] + m_2 l_{c2} cos[q_1(t) + q_2] \\ m_2 l_{c2} cos[q_1(t) + q_2] \end{bmatrix} = \begin{bmatrix} \tau_1(t) \\ 0 \end{bmatrix} \tag{28}$$

Pre-multiplication of both sides of Equation (28) by a matrix

$$\begin{bmatrix} I_1 + I_2 & I_2 \\ I_2 & I_2 \end{bmatrix}^{-1} = \begin{bmatrix} \frac{1}{I_1} & -\frac{1}{I_1} \\ -\frac{1}{I_1} & \frac{1}{I_1} + \frac{1}{I_2} \end{bmatrix} \tag{29}$$

yields

$$\ddot{q}(t) + \dot{q}_1(t) m_2 l_1 l_{c2} sin[q_2] \begin{bmatrix} 0 & \frac{1}{I_1} \\ \frac{1}{I_2} & -\frac{1}{I_1} \end{bmatrix} \dot{q}(t) + g \begin{bmatrix} \frac{1}{I_1} & -\frac{1}{I_1} \\ -\frac{1}{I_1} & \frac{1}{I_1} + \frac{1}{I_2} \end{bmatrix} \begin{bmatrix} (m_1 l_{c1} + m_2 l_1) cos[q_1(t)] + m_2 l_{c2} cos[q_1(t) + q_2] \\ m_2 l_{c2} cos[q_1(t) + q_2] \end{bmatrix} = \begin{bmatrix} \tau_1(t) \\ 0 \end{bmatrix} \tag{30}$$

Further transformations lead to

$$\begin{bmatrix} \ddot{q}_1(t) \\ 0 \end{bmatrix} + m_2 l_1 l_{c2} sin(q_2) \begin{bmatrix} 0 \\ \frac{\dot{q}_1^2(t)}{I_2} \end{bmatrix} + g \begin{bmatrix} \frac{(m_1 l_{c1} + m_2 l_1) cos[q_1(t)]}{I_1} \\ \frac{(m_1 l_{c1} + m_2 l_1) cos[q_1(t)]}{I_1} + \frac{m_2 l_{c2} cos[q_1(t) + q_2]}{I_2} \end{bmatrix} = \begin{bmatrix} \tau_1(t) \\ 0 \end{bmatrix} \tag{31}$$

From the first row, one has

$$\ddot{q}_1(t) + \frac{g(m_1 l_{c1} + m_2 l_1) cos[q_1(t)]}{I_1} = \tau_1(t)$$

Additionally, the second row must be satisfied

$$\frac{m_2 l_1 l_{c2} sin(q_2)}{I_2} \dot{q}_1^2(t) + \frac{g(m_1 l_{c1} + m_2 l_1) cos[q_1(t)]}{I_1} + \frac{g m_2 l_{c2} cos[q_1(t) + q_2]}{I_2} = 0 \tag{32}$$

As a discrete time, mathematical model, one takes an approximation of the derivative by a difference

$$\frac{q_1(kh) - 2q_1(kh - h) + q_1(kh - 2h)}{h^2} + \frac{g(m_1 l_{c1} + m_2 l_1) cos[q_1(kh)]}{I_1} = \tau_1(kh) \tag{33}$$

In further considerations to verify adopted assumptions, only the first link was the subject of the analysis. Mechanical friction and backlash are omitted. Now one denotes:

$$K = \frac{g(m_1 l_{c1} + m_2 l_1)}{I_1} \tag{34}$$

Hence, under the assumptions mentioned above, in the model there is only one parameter to evaluate.

4.2. Variable Fractional-Order Mathematical Model (VFOM) of the Robot Arm

The VFOBD may will be applied to model the robot arm. From the general form of a linear, time-invariant variable fractional-order difference equation:

$$\sum_{i=0}^{n} A_{i0}{}^{GL}\Delta_k^{(\nu_k)} y_k = \sum_{i=0}^{m} B_{i0}{}^{GL}\Delta_k^{(\mu_k)} u_k \tag{35}$$

where

A_i, B_j—constant coefficients with $A_n = 1$,
$\nu_{n,k} > \nu_{n-1,k} > \cdots > \nu_{1,k} > \nu_{0,k} = 0$—order functions,
$\mu_{m,k} > \mu_{m-1,k} > \cdots > \mu_{1,k} > \mu_{0,k} \geq 0$—order functions,
u_k, y_k—the robot arm input and output functions.

The robot arm possesses the integration element properties. Hence, in the first approach one considers (14) with $n = 1, m = 0$ and $\mu_k = 0$. Then, from (35) one gets the equation:

$$_0^{GL}\Delta_k^{(\nu_k)} y_k = B_0 u_k \tag{36}$$

describing a variable fractional-order integrator (VFO-I) [25]. In such simple model structure, there are two parameters to select: a coefficient B_0 and an order function ν_k. Note that this is a generalization of the FO discrete integrator, which in turn is a generalization of the classical (first-order) integrator. By (10) and (11), a response of the VFO-I is of the form:

$$y_k = -\begin{bmatrix} a_1^{(\nu_k)} & a_2^{(\nu_k)} & \cdots & a_k^{(\nu_k)} \end{bmatrix} \begin{bmatrix} y_{k-1} \\ y_{k-2} \\ \vdots \\ y_0 \end{bmatrix} + B_0 u_k \tag{37}$$

It is easy to prove that Equation (37) can be transformed to an equivalent form

$$y_k = B_0{}_0^{GL}\Delta_k^{(\mu_k)} u_k \tag{38}$$

where

$$\mu_k = -\nu_k$$

Because one may expect non-linear behavior, one takes that $B_0(u_k)$. For a better modelling elasticity, one also assumes that the integration order depends on the input signal. Hence, the final model structure has the form:

$$y_k = B_0(u_k)_0^{GL}\Delta_k^{[\mu_k(u_k)]} u_k \tag{39}$$

The block diagram of the Wiener VFOM is presented in Figure 13.

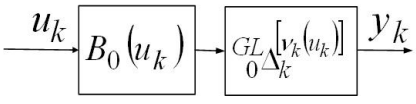

Figure 13. Block diagram of the VFOM.

5. The Robot Arm Tests

The examined system is part of a larger project, which is the development of a comprehensive design of the mobile platform. Figure 14 shows the executive part of the robot with an observation head. The drive in this mechanism is carried out by means of a DC electric drive motor with harmonic gear powered by a single-phase PWM inverter. Positive feedback to the inverter occurs with a delay of one trial period.



Figure 14. Robot arm photo.

To the robot arm electrical drive input, several constant voltages were supplied. Zero initial conditions were assumed although the initial angle is nonzero. This is caused by the robot construction. Hence, there were measured step responses of the robot arm. The input constant voltages are collected in a set $\mathbb{U}$:

$$\mathbb{U} = \{3, 4, 5, 6, 7, 8, 9, 10, 15, 20, 25\} \text{ [V]} \tag{40}$$

The responses are presented in Figure 15. It can be seen in Figure 15 that higher input voltages cause the faster responses of the robot arm.

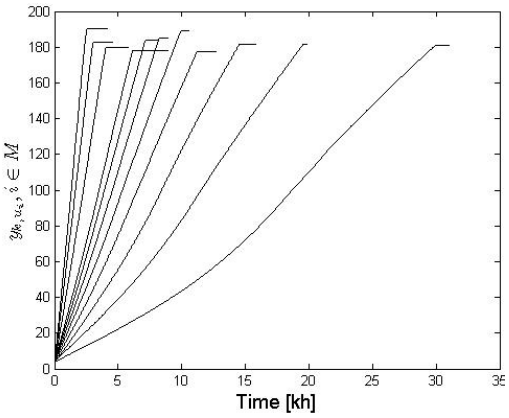

Figure 15. Robot arm measured step responses.

6. The VFOM and CM Parameters Selection

In this Section, both models' parameter selection methods are described. The main fitting criterion is a minimum of the square error defined as a difference between measured real system responses $y_{m,k}$ and simulated $y_{s,k}$ ones

$$I_{CM} = \min_{K,[0\ k]} \left| y_{m,k} - y_{s,k}(K) \right|^2 \tag{41}$$

$$I_{VFOM} = \min_{B_0,\nu_k,[0\ k]} \left| y_{m,k} - y_{s,k}(B_0, \nu_k) \right|^2 \tag{42}$$

First, the coefficient B_0 in formula (36) is evaluated. Here, one initially assumes that $\nu_k = 1$. Then, for $u_k = u_0 1_k$ (1_k denotes the unit discrete step function) one gets

$$y_{j,k} = B_0 \sum_{i=0}^{k} u_i = B_0 u_{j,0} kh \ for \ u_{j,0} \in \mathbb{U} \tag{43}$$

where h denotes a sampling time. For the chosen time instants (for which the responses achieve for the first time its maximal value) from (43) one gets coefficients

$$B_{j,0}(u_{j,0}) = \frac{y_{k_{max}}}{u_{j,0}k_{max}h} \; for \; u_{j,0} \in \mathbb{U} \tag{44}$$

Plots of $B_{j,0}(u_{j,0})y_{j,k}$ are presented in Figure 16. The coefficients (44) are plotted in Figure 17.

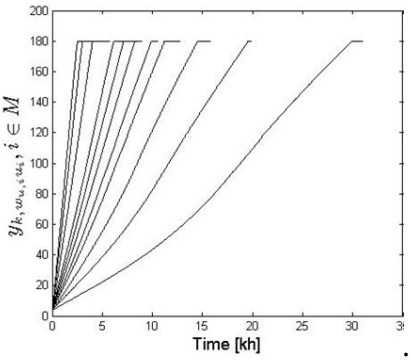

Figure 16. Robot arm measured step responses with coefficients (44).

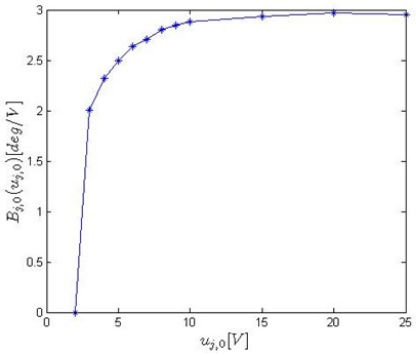

Figure 17. Plot of coefficients $B_{j,0}\left(u_{j,0}\right)$.

This enables us to evaluate the static characteristic of the model. It is presented in Figure 18. To check the response shapes, the time coefficients are added. The coefficients $w_j(u_{j,0})$ are selected in order to get the same transient times. Comparison of all such responses revealed its changes due to the input signal value. In Figure 18 all mentioned responses are presented.

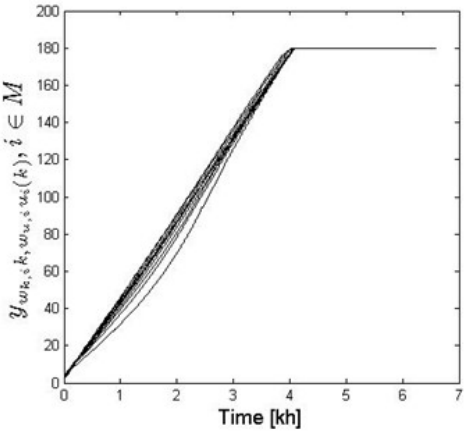

Figure 18. Responses of the robot arm with transformed time.

As the order functions, one takes

$$v_k = -1 + c(u_k)e^{dk} \tag{45}$$

with $0 < c(u_k) < 1, d < 0$. For $c(u_k)$ and d parameters, selection of an ISE (integrated square error) criterion was applied.

$$I[c(u_k), d] = \sum_{i=0}^{k_{max}} e_i^2 \tag{46}$$

where

$$e_k = y_k - y_{s,k} = y_k - B_0(u_k)_0^{GL}\Delta_k^{[-1+c(u_k)e^{dk}]}u_k \tag{47}$$

For $0 < c(u_k) < 1$, a plot of coefficients $c(u_k)$ vs. u_k is presented in Figure 19.

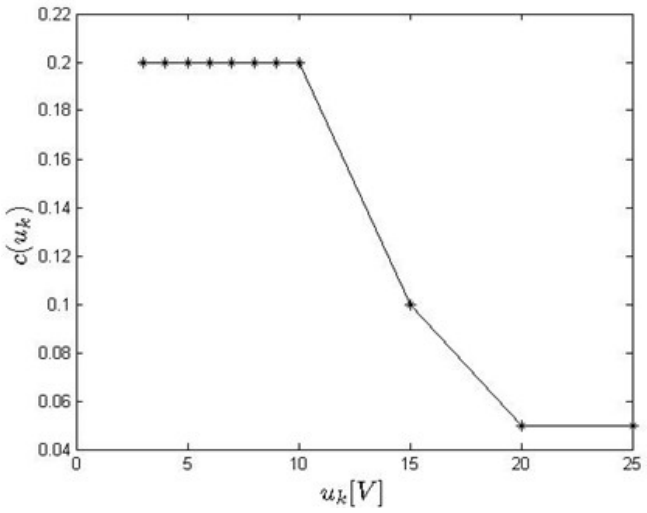

Figure 19. Coefficient $c(u_k)$ vs. u_k.

The responses that were measured and simulated for $d = -0.001$ are presented in Figure 20. Figure 20 also shows the response obtained by simulation of the classical model where $\frac{g(m_1 l_{c1} + m_2 l_1)}{I_1} = 0.6$ and $K = 0.1787$ are added (in blue).

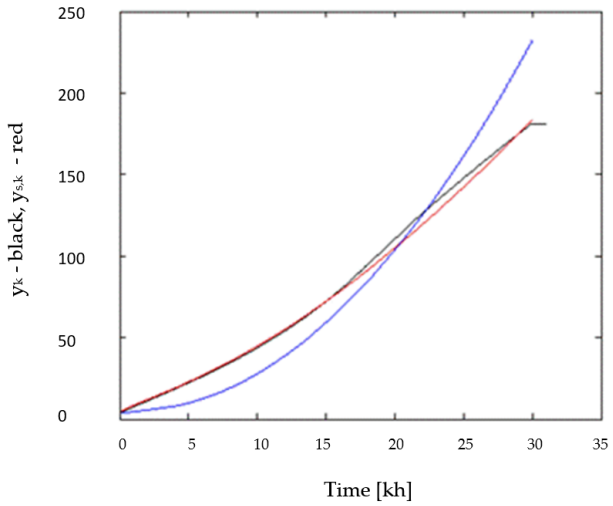

Figure 20. Measured (black) and simulated fractional (red) and classical (blue) robot arm mathematical model step responses.

In Figure 21, similar responses for different input signals are compared.

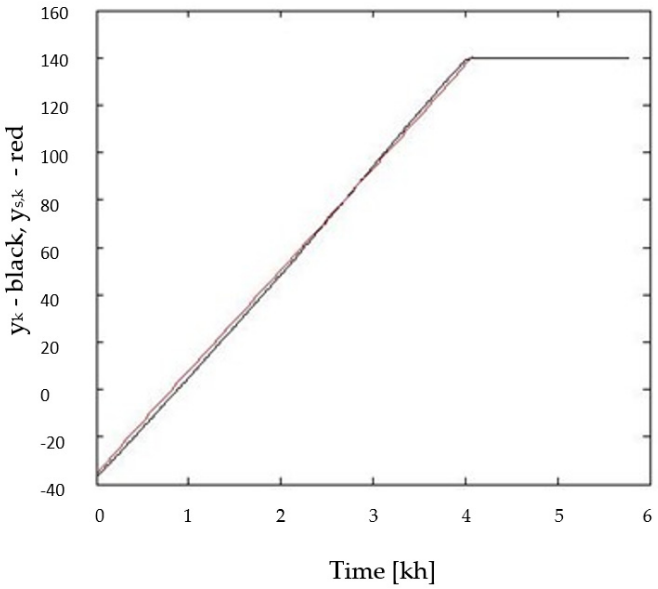

Figure 21. Measured (black) and simulated fractional model (red) robot arm responses.

To compare the simulation results, two performance criteria were used: IAE and ISE. The first error is defined by formula (45) and the second is defined as $e_k = y_k - q_1(\mathrm{kh})$ where $h = 0.0215$ denotes the simulation step. The obtained IAE and ISE criteria values are given in Figure 22.

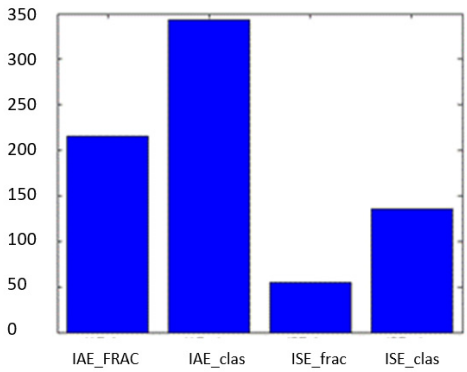

Figure 22. IAE and ISE criteria.

7. Conclusions

In this article, two mathematical models of a robot arm were analyzed: one derived from the well-known Newton–Euler formalism, and the second described by variable fractional-order difference equations. Both models were compared with measured values of a robot arm. Based on the two criteria used for comparison (IAE and ISE), it was shown that the model described by variable fractional-order difference equations gave better result. The proposed variable fractional-order difference equation-based model had more parameters than the classical one, which led to a better model of the actual behavior of the modeled object. The open question is the selection of the right order function, which can be related to the measured real-time signals in the system. The next step is also to investigate the impact of platform movement on the tested system. In the real model, the actuator in the form of an arm is mounted on a six-wheel mobile platform with independent suspension of each wheel. We intend to develop the model with elements of the dynamics

of the platform's movement (change in speed and direction of movement, impact of ground shape, etc.) on the robot arm.

Author Contributions: P.O. conceived the research direction and collected relevant information; P.O., P.D. and M.B. designed the Simulink and Matlab simulations and experiment; M.B. built the test stand; P.D. provided microcontroller implementation; P.O., M.B. and P.D. analyzed the data; P.O., M.B., and P.D. wrote the paper. All authors have read and agreed to the published version of the manuscript.

Funding: This research received no external funding.

Institutional Review Board Statement: Not applicable.

Informed Consent Statement: Not applicable.

Data Availability Statement: Data sharing not applicable.

Conflicts of Interest: The authors declare no conflict of interest.

References

1. Govindarajan, V.; Bhattacharya, S.; Kumar, V. Human-robot collaborative topological exploration for search and rescue applications. In *Distributed Autonomous Robotic Systems*; Springer: Tokyo, Japan, 2016; pp. 17–32.
2. Brito, T.; Queiroz, J.; Piardi, L.; Fernandes, L.A.; Lima, J.; Leitão, P. A machine learning approach for collaborative robot smart manufacturing inspection for quality control systems. *Procedia Manuf.* **2020**, *51*, 11–18. [CrossRef]
3. Kilbas, A.A.; Srivastava, H.; Trujillo, J.J. *Theory and Applications of Fractional Differential Equations*; Elsevier Science Inc: New York, NY, USA, 2006; Volume 204. [CrossRef]
4. Podlubny, I. Fractional Differential Equations. In *An Introduction to Fractional Derivatives, Fractional Differential Equations, to Methods of Their Solution and Some of Their Applications*; Academic Press: San Diego, CA, USA, 1999.
5. Sabatier, J. Fractional order systems. Applications in modelling, identification, and control. *J. Eur. Des. Systèmes Automatisés. RS Série JESA* **2008**, *42*, 625.
6. Spong, M.W.; Vidyasagar, M. *Robot Dynamics, and Control*; John Wiley & Sons, Inc.: Hoboken, NJ, USA, 1989.
7. Alagoz, B.B.; Tepljakov, A.; Ates, A.; Petlenkov, E.; Yeroglu, C. Time-domain identification of One Noninteger Order Plus Time Delay models from step response measurements. *Int. J. Model. Simul. Sci. Comput.* **2019**, *10*, 1941011. [CrossRef]
8. Garrappa, R.; Kaslik, E.; Popolizio, M. Evaluation of Fractional Integrals and Derivatives of Elementary Functions: Overview Tutorial. *Mathematics* **2019**, *2*, 7050407. [CrossRef]
9. Vinagre, B.M.; Podlubny, I.; Hernandez, A.; Feliu, V. Some approximations of fractional order operators used in control theory and applications. *Fract. Calc. Appl. Anal.* **2000**, *3*, 231–248.
10. Rosario, J.M.; Didier, D.; Tenreiro Machado, J.A. Analysis of fractional-order robot axis dynamics. *IFAC Proc.* **2006**, *39*, 367–372. [CrossRef]
11. Rhouma, A.; Sami, H. A Microcontroller Implementation of Fractional Order Controller. *Int. J. Contr. Syst. Robot.* **2017**, *2*, 122–127.
12. Sierociuk, D.; Malesza, W. Fractional variable order anti-windup control strategy. *Bull. Pol. Acad. Sci. Tech. Sci.* **2018**, *66*, 427–432.
13. Samko, S.; Ross, B. Integration and differentiation to a variable fractional order. *Integr. Transf. Spec. Funct.* **1993**, *1*, 277–300. [CrossRef]
14. Sheng, H.; Sun, H.G.; Coopmans, C.; Chen, Y.Q.; Bohannan, G.W. A physical experimental study of variable-order fractional integrator and differentiator. *Eur. Phys. J. Spec. Top.* **2011**, *193*, 93–104. [CrossRef]
15. Meng, R.; Yin, D.; Drapaca, C.S. A variable order fractional constitutive model of the viscoelastic behavior of polymers. *Int. J. Non-Linear Mech.* **2019**, *113*, 171–177. [CrossRef]
16. Sierociuk, D.; Macias, M. Comparison of variable fractional order PID controller for different types of variable order derivatives. In Proceedings of the 14th International Carpathian Control Conference (ICCC), Rytro, Poland, 26–29 May 2013; pp. 334–339. [CrossRef]
17. Ostalczyk, P. Variable-, fractional-order discrete PID controllers. In Proceedings of the 2012 17th International Conference on Methods & Models in Automation & Robotics (MMAR), Miedzyzdroje, Poland, 27–30 August 2012; pp. 534–539. [CrossRef]
18. Dabiri, A.; Moghaddam, B.P.; Machado, J.T. Optimal variable-order fractional PID controllers for dynamical systems. *J. Comput. Appl. Math.* **2018**, *339*, 40–48. [CrossRef]
19. Ostalczyk, P.; Duch, P. Closed—Loop system synthesis with the variable-, fractional—Order PID controller. In Proceedings of the 2012 17th International Conference on Methods & Models in Automation & Robotics (MMAR), Miedzyzdroje, Poland, 27–30 August 2012. [CrossRef]
20. Oziablo, P.; Mozyrska, D.; Wyrwas, M. Discrete-Time Fractional, Variable-Order PID Controller for a Plant with Delay. *Entropy* **2020**, *22*, 771. [CrossRef] [PubMed]
21. Liu, L.; Pan, F.; Xue, D. Variable-order fuzzy fractional PID controller. *ISA Trans.* **2015**, *55*, 227–233. [CrossRef] [PubMed]

22. Amini, M.; Waezi, Z.; Manthouri, M. Seismic control of the structures with active tuned mass damper and variable fractional order fuzzy proportional–integral–derivative controller. *J. Vib. Control.* **2022**, 10775463221115451. [CrossRef]
23. Ostalczyk, P.; Brzezinski, D.; Duch, P.; Łaski, M.; Sankowski, D. The variable, fractional-order discrete-time PD controller in the IISv1. 3 robot arm control. *Open Phys.* **2013**, *11*, 750–759. [CrossRef]
24. Ostalczyk, P.W.; Duch, P.; Brzeziński, D.W.; Sankowski, D. Order functions selection in the variable-, fractional-order PID controller. In *Advances in Modelling and Control of Non-Integer-Order Systems*; Springer: Cham, Switzerland; pp. 159–170.
25. Ostalczyk, P. Zarys rachunku różniczkowo—Całkowego ułamkowych rzędów. In *Teoria i zastosowanie w automatyce, Komitet Automatyki i Robotyki Polskiej Akademii Nauk, Wydawnictwo Politechniki Łódzkiej. Monografie Tom 12*; Łódź, Polska, 2008. Available online: http://repozytorium.p.lodz.pl/handle/11652/1843 (accessed on 28 January 2023).
26. Ostalczyk, P. Discrete Fractional Calculus. In *Applications in Control and Image Processing, Series in Computer Vision*; World Scientific: Hackensack, NJ, USA, 2015; Volume 4, ISSN 2010-2143.
27. Sierociuk, D.; Macias, M.; Malesza, W.; Sarwas, G. Dual Estimation of Fractional Variable Order Based on the Unscented Fractional Order Kalman Filter for Direct and Networked Measurements. *Circuits Syst. Signal Process.* **2016**, *35*, 2055–2082. [CrossRef]
28. Monje, C.A.; Chen, Y.; Vinagre, B.M.; Xue, D.; Feliu, V. Fractional-order Systems and Controls Fundamendals and Applications. In *Advances in Industrial Control*; Springer: London, UK, 2010.

Disclaimer/Publisher's Note: The statements, opinions and data contained in all publications are solely those of the individual author(s) and contributor(s) and not of MDPI and/or the editor(s). MDPI and/or the editor(s) disclaim responsibility for any injury to people or property resulting from any ideas, methods, instructions or products referred to in the content.